Effect of low loading of yttrium on Ni-based layered double hydroxides in CO_2 reforming of CH_4

Katarzyna Świrk[1,2,*], Monika Motak[2], Teresa Grzybek[2], Magnus Rønning[3], Patrick Da Costa[1]

[1]Sorbonne Université, CNRS, Institut Jean le Rond d'Alembert, F-78210 Saint-Cyr l'École, France
[2]AGH University of Science and Technology, Department of Fuel Technology, 30-059 Cracow, Poland
[3]Norwegian University of Science and Technology, Department of Chemical Engineering, N-7491 Trondheim, Norway

Abstract

Ni/Al/Mg layered double hydroxides (LDHs) modified with low loading of yttrium (0.2 and 0.4 wt%) were used in dry reforming of methane at 700 °C. Physicochemical characterization, such as: X-ray fluorescence, N_2 sorption, X-ray diffraction, temperature programmed reduction in H_2, temperature programmed desorption of CO_2, H_2 chemisorption, thermogravimetry analysis coupled by mass spectrometry and Raman spectroscopy, showed that the introduction of low loadings of yttrium lead to a smaller Niº crystallite size, a decrease in reducibility of the nickel, and a decreased number of basic sites in the modified Ni/LDHs catalysts**.** The doping with 0.4 wt% of Y improves catalytic activity resulting in higher CH_4 and CO_2 conversions at 700 °C, i.e. ca. 84 % and ca. 87 %, respectively with no clear deactivation observed after 5 h run. The increase in CO_2 conversion and a decrease of H_2/CO ratio indicates that side reactions occurs during DRM.

Keywords: dry reforming of methane, nickel, yttrium, layered double hydroxides

*Corresponding author: Katarzyna Świrk (swirk@agh.edu.pl , katarzyna.swirk@sorbonne-univeriste.fr)

1. Introduction

With a view to enhancing chemical CO_2 utilization technologies, dry methane reforming (DRM) is a one of the prospective processes, which allows to convert carbon dioxide and methane into valuable products, i.e. synthesis gas (equation 1). The process is complex and consists of several steps, in which the most important are the reactions mentioned below [1,2]:

$$CH_4 + CO_2 = 2CO + 2H_2\,, \qquad \Delta H^{\theta} = 247\ \text{kJ/mol} \qquad (1)$$

$$CO_2 + H_2 = H_2O + CO\,, \qquad \Delta H^{\theta} = 41\ \text{kJ/mol} \qquad (2)$$

$$2CO = C_{(s)} + CO_2\,, \qquad \Delta H^{\theta} = -172\ \text{kJ/mol} \qquad (3)$$

$$CH_4 = C_{(s)} + 2H_2\,, \qquad \Delta H^{\theta} = 75\ \text{kJ/mol} \qquad (4)$$

The industrialization of DRM is, however, limited by a high reaction temperature (at least 642 °C), which increases the economic costs of process, and by undesirable coke formation (equations 3 and 4) which causes the catalyst deactivation [3]. Supported noble metal catalysts (Rh, Ru, Ir, Pt and Pd) show efficient catalytic performance and low sensitivity to carbon deposits, but their high price and low availability prevent their industrial application in contrast to Ni-based catalysts. The latter represent a promising alternative [4–7]. However, the main drawback of their application is fast deactivation caused by coke formation, sintering of active phase and metal oxidation [2,8,9]. The deactivation may be limited due to possible improvement of the physical properties, e.g. Ni particle size lower than 10 nm and high dispersion of the metal species [10,11]. Thus, finding a highly active, selective and stable catalyst remains a serious problem for industrialization of DRM and the preparation of a novel catalyst is still a challenge [12,13]. The choice of proper support may contribute to an improvement.

Synthetic layered double hydroxides (LDHs), show good properties as precursors due to their double layered and homogenous structure with appropriate basic properties and the presence of Mg^{2+} and Al^{3+} introduced by co-precipitation method. These cations may by

partially substituted by ions of promoter, in order to improve properties of the material [14–17].

A large number of studies have shown that Ni-based catalysts can result in high activity and stability in DRM [18–27].

Yttrium has received considerable attention as a promising promoter for many chemical processes [28–33], including dry reforming of methane [34–37]. Recently, yttrium promotion (0.2-0.6 wt%) was examined by us over Ni-based catalysts, which were additionally modified with Zr [33]. The promotion with Zr (5 wt%) and Y (0.4 wt%) resulted in an enhanced stability and activity which could be ascribed to the formation of ZrO_2-Y_2O_3, the latter possibly leading to the reduction of bulk NiO. Bellido et al. [38] also synthesized Zr-modified Ni-containing catalysts with a varying mole fraction of Y (4 to 12 mol%). The catalyst modified with 8 mol% showed the highest activity and stability in the DRM, possibly due to the increased formation of oxygen vacancies. The effect of higher Y-loadings (0.6 and 1.5 wt%) on Ni/Mg/Al layered-double hydroxides was also studied elsewhere [3]. The modification with these quantities resulted in the increased specific surface area, smaller Ni crystallite size, enhanced dispersion of active sites, changes in the reducibility and higher distribution of weak and medium basic sites as compared to the unpromoted catalyst. The modification with higher amount of yttrium (1.5 wt%) showed enhanced stability in the dry reforming of methane tests.

No study concerning the effect of low yttrium loading (lower than 0.6 wt%) on Ni-LDHs has been reported before. Thus, the aim of this work was to examine the influence of the yttrium promotion (0.2 and 0.4 wt%) of Ni-based layered double-hydroxides on their structure and catalytic behavior in dry reforming of methane.

2. Experimental

2.1. Catalysts preparation

The layered double hydroxides were synthesized by co-precipitation method. An aqueous solution of following salts was used: $Mg(NO_3)\cdot 6H_2O$ (Sigma Aldrich, 99% pure), $Ni(NO_3)_2\cdot 6H_2O$ (Sigma Aldrich, 98.5% pure), $Al(NO_3)_2\cdot 9H_2O$ (Fluka, 98% pure) and $Y(NO_3)_3\cdot 6H_2O$ (Aldrich, 99.8% pure), together with a 2M solution of NaOH to control pH. These two solutions have been added dropwise to sodium carbonate solution (cp=25%). The pH of a mixture was kept in the range of 9.8-10.2. The synthesis of the materials assumed ratio M^{2+}/M^{3+}=3.0. In individual sample the following content of yttrium was doped 0.2 and 0.4 wt%. After co-precipitation of the salts, the mixture was aged for 24 h, and the slurry was then filtered and washed with distilled water. The final product was calcined in air at 550 ºC for 5 h. So prepared catalysts were labeled HTNi, HTNi-Y0.2 and HTNi-Y0.4.

2.2. Catalysts characterization

X-Ray Fluorescence (XRF) analysis was used to examine elemental composition in the Ni catalysts after calcination. The analysis was carried out by using a Supermini200 instrument. The samples were kept under vacuum at 36.5 °C in the presence of P-10 gas (flow 24.7 cm^3/min). The powdered materials were diluted in boric acid and pelletized under a press (10 bar). The pellets were covered with 6 μm polypropylene film.

Nitrogen sorption was performed by a Micromeritics TriStar II 3020 in order to determine textural properties of the materials. The samples were degassed for 3 h at 110 °C before the measurement. Nitrogen sorption isotherms were measured at liquid-nitrogen temperature of -195 °C.

X-ray diffraction (XRD) patterns were obtained from PANalytical-Empyrean diffractometer, equipped with CuKα (λ = 0.15406 nm) radiation source. The average crystallite size of Ni was determined from the Scherrer equation.

Temperature-programmed reduction (TPR-H_2) measurements were carried out on a BEL Japan BELCAT-M equipped with a thermal conductivity detector (TCD). Calcined materials (60 mg) were first degassed in helium atmosphere at 100 °C for 2 h and then reduced in 5 % H_2/Ar mixture with a heating rate of 10 °C/min starting from 100 °C to 900 °C. The measurements of temperature programmed desorption (TPD-CO_2) were performed for the sample just after TPR-H_2 test, using the same apparatus. CO_2 was adsorbed at 80 °C for 1 h from a mixture of 10% CO_2/He. Then, helium flow was applied for 15 min in order to desorb weakly adsorbed CO_2. Finally, the materials were heated from 80 °C to 800 °C in helium in order to determine weak, medium and strong basic sites based on temperature of desorption. TPD profiles were deconvoluted into three Gaussian peaks.

Hydrogen chemisorption was used to determine nickel dispersion (Micromeritics, ASAP 2020S). 200 mg of calcined materials were loaded in tubular quartz reactor. Prior the experiments, evacuation at 40 °C for 1 h and reduction in pure H_2 at 900 °C for 1 h was applied. After the reduction, the sample was evacuated in helium for 30 min at 900 °C and subsequently for 1 h at 40 °C. After the leak test pass, the sample was continuously evacuated for 30 min at 40 °C, at this temperature, an adsorption isotherm was recorded and the metal dispersion was determined based on the quantity of hydrogen uptake. Also, Ni crystallite size was calculated, assuming spherical metal crystallites of uniform diameter *d* [39]:

$$d = \frac{97.1}{\%D} \qquad \text{[nm]} \qquad (5)$$

In which *97.1* represents a constant for nickel and *%D* the percentage dispersion obtained from H_2 chemisorption.

Thermogravimetric analyzes were carried out by a TGA-MS (TGA: Netzsch STA 449C Jupiter, MS: Netzsch Aërlos QMS 403C) in order to evaluate the coke formation on spent catalysts. An air flow of 100 cm^3/min and protective gas flow of 20 cm^3/min were applied. 10 mg of a spent sample was heated starting from ambient temperature to 900 °C with a ramp rate of 10 °C/min. The amount of coke deposition was estimated by the mass loss in TGA analysis, confirming by CO_2 production derived from MS results.

Raman was employed to characterize carbon deposits formed on the spent catalysts by using a Horiba Jobin Yvon LabRam HR800 instrument. The spectra were recorded with a laser excitation wavelength of 633 nm at an accumulation of 3 and an acquisition time of 20 s. A diffraction grating of 1800 gr/mm and a 50x objective were applied.

2.3. Catalytic tests

The catalytic DRM tests were conducted under atmospheric pressure, in a fixed-bed U type reactor (8 mm inner diameter). The catalytic bed temperature was monitored by a K-type thermocouple placed in a quartz shield. Calcined catalysts were introduced into the reactor and reduced in situ earlier to the reaction in flowing a mixture of 5% H_2/Ar (flow 50 cm^3/min) at 900 °C for 1 h to activate the catalyst in-situ. Then two types of tests were carried out.

A first series of the experiments were performed in the temperature range of 850-600 °C with a temperature step every 50 °C, and cooling time of 15 min between the steps. The duration of the test at each temperature was 30 minutes corresponding to steady-state measurements.

A second series of experiments were carried out in isothermal conditions at 700 °C for 5 hours in order to evaluate the catalysts initial stability.

For both experiments, the gas composition was equal to CH_4/CO_2/Ar= 1/1/8. The total flow was 100 cm^3/min which corresponds to a gas hourly space velocity (GHSV) of 20,000 h^{-1}. The outlet gases were analyzed by gas chromatograph (490 Varian Micro-GC). In order to acquire

CH_4, CO_2, conversions as well as the H_2/CO ratios the following equations (6), (7), (8) were employed:

$$X_{CH_4} = \left[\frac{n_{CH_4^{in}} - n_{CH_4^{out}}}{n_{CH_4^{in}}} \right] \cdot 100 \qquad [\%] \qquad (6)$$

$$X_{CO_2} = \left[\frac{n_{CO_2^{in}} - n_{CO_2^{out}}}{n_{CO_2^{in}}} \right] \cdot 100 \qquad [\%] \qquad (7)$$

$$H_2/CO = \left[\frac{n_{H_2^{out}}}{n_{CO^{out}}} \right] \qquad (8)$$

Direct methane decomposition (DMD) was also carried out in the same experimental device. The following gas composition was equal to CH_4/Ar= 2/8. The total flow was 100 cm^3/min which corresponds to a gas hourly space velocity (GHSV) of 20,000 h^{-1}. Similarly, to equation (6), CH_4 conversion was calculated as follows:

$$X_{DMD,CH_4} = \left[\frac{n_{CH_4^{in}} - n_{CH_4^{out}}}{n_{CH_4^{in}}} \right] \cdot 100 \qquad [\%] \qquad (9)$$

3. Results and discussion

3.1. Catalysts characterization

Elemental analysis was carried out by means of X-ray fluorescence (XRF). The contents of Ni and Y, together with the assumed M^{2+}/M^{3+} ratio are listed in Table 1. The studied catalysts showed ca. 20 wt% of Ni loading, and yttrium contents which are close to the nominal values, i.e. 0.2 and 0.4 wt%. The calculated ratios of M^{2+}/M^{3+}, i.e. (Ni,Mg)/(Al,Y), were also close to the values which were assumed during the synthesis step. This shows that the studied materials were successfully synthesized, and contents of metals may be easily controlled during the material preparation.

Table 1 Summary of the structural properties of the calcined catalysts. The values in brackets are nominal values.

Catalyst	XRF			Nitrogen sorption		
	Ni^{2+} [wt%]	Y^{3+} [wt%]	M^{2+}/M^{3+} [-]	S_{BET} [m^2/g] [1)]	V_p [cm^3/g] [2)]	d_p [nm] [3)]
HTNi	20	-	3.6 (3.0)	120	0.6	19
HTNi-Y0.2	19	0.2 (0.2)	3.2 (3.0)	127	0.5	16
HTNi-Y0.4	21	0.4 (0.4)	3.5 (3.0)	120	0.5	15

[1)] specific surface areas calculated from the BET equation

[2)] mesopore volumes derived from the BJH desorption isotherm

[3)] pore size distribution obtained from the BJH desorption isotherm

Specific surface area for calcined samples was obtained through BET analysis, and varied from 120 to 127 m^2/g, suggesting no significant influence of yttrium addition on this parameter (Table 1). Total pore volume also remained stable after modification with yttrium. However, pore diameters slightly decreased as compared to HTNi catalyst. Fig. 1 shows IV type isotherms for the calcined materials, which are characteristic for mesoporous structure. [40] The obtained hysteresis loop indicates the slit shaped pores with nonuniform size and shape. The adsorbed amounts decreased with the increasing loading of yttrium, which may possibly be related with observed decrease in pore size (Fig. 2).

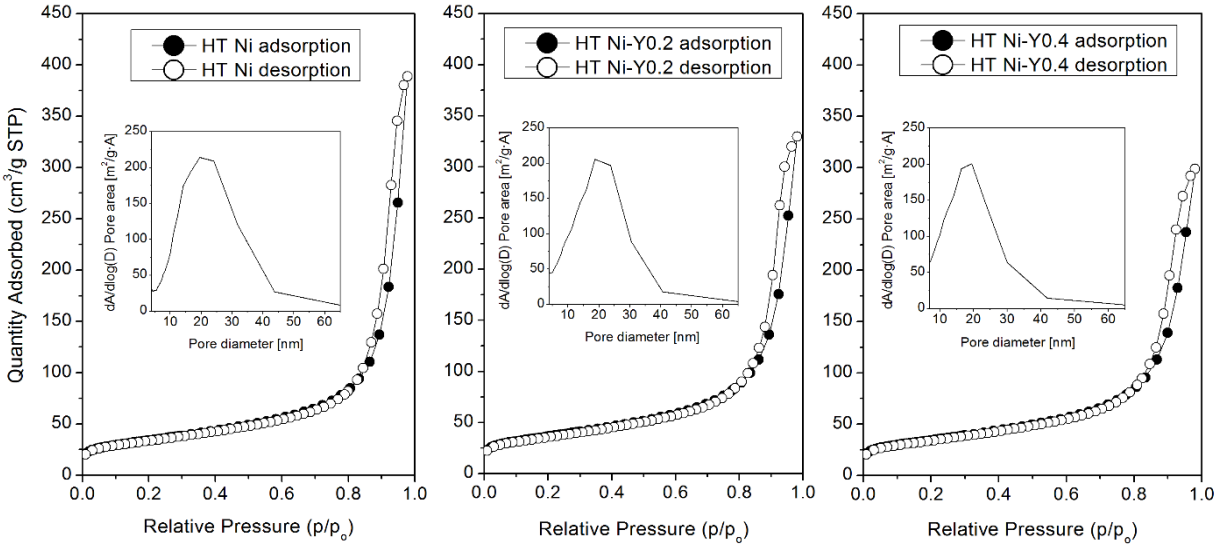

Fig. 1 N_2 adsorption/desorption isotherms and pore distribution for HTNi, HTNi-Y0.2 and HTNi-Y0.4 catalysts.

Fig. 2A presents XRD patterns of the prepared catalysts. For the calcined samples reflections of Ni-Mg-Al mixed oxides (ICOD 00-045-0946) (2θ ca. 36.7 º, 43 º, 62.5 º) are observed, which are characteristic for layered double-hydroxides after thermal treatment at 550 ºC [11,41,42]. The reduction at 900 ºC resulted in the formation of segregate phase of metallic nickel (ICOD 01-087-0712) as evidenced by reflections at 2θ ca. 44.5 º, 52 º, 76.5 º corresponding to crystal planes of (111), (200), (220), respectively (Fig. 2B) [3,31,41]. No separate phase for yttrium was registered in XRD patterns, probably due to small amounts of this metal [3]. Moreover, according to Li et al.[43] and Taherian et al.[32] promotion with $Y(NO_3)_3 \cdot 6H_2O$ resulted in Y_2O_3 phase formation which is not further unreducible in our tested conditions. The Ni° crystallite sizes calculated from the width of the reflection at 2θ of ca. 53°, are shown in Table 2. The yttrium addition resulted in a decrease of nickel crystallites from ca. 8 nm for the unpromoted HTNi to ca. 5-6 nm for HTNi-Y (Table 2).

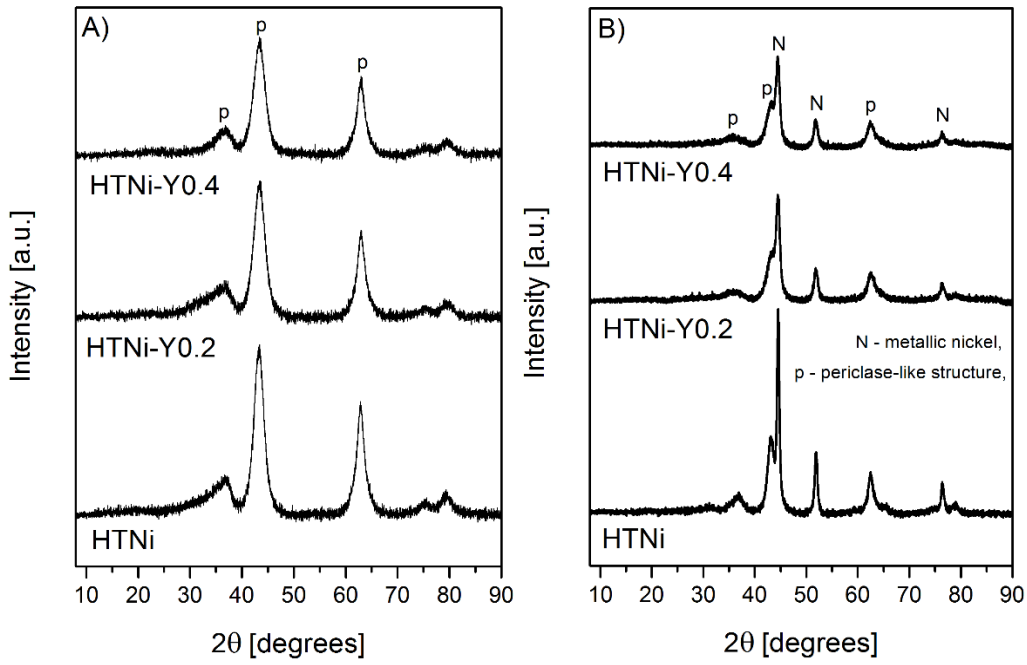

Fig. 2 XRD patterns of a) catalysts after calcination at 550 °C for 5 h, b) catalysts reduced in 5% H_2/Ar mixture at 900 °C for 1 h (GHSV= 20,000 h^{-1}).

Table 2 Nickel crystallite size and metal dispersion for the reduced catalyst, and reducibility and basic properties of the studied catalysts.

Catalyst	XRD	H_2 chemisorption		TPR-H_2	TPD-CO_2			
	Ni^o crystallite size [1] [nm]	Ni^o crystallite size [2] [nm]	Dispersion Ni [%]	H_2 consumption [mmol H_2/g]	Number of basic sites [μmol/g]			
					Weak	Medium	Strong	Total basicity
HTNi	8	11	8.9	0.209	16	44	46	107
HTNi-Y0.2	6	10	9.5	0.143	12	32	19	63
HTNi-Y0.4	5	9	10.7	0.151	16	20	23	59

[1] Based on the Scherrer equation, from the width at half-maximum of the XRD reflections at 2Θ ca. 53°.

[2] From H_2 chemisorption assuming spherical crystallites of uniform size, calculated from equation (5).

The reducibility of the catalysts was studied by TPR-H_2. Hydrogen consumption for the reduced samples, presented in Table 2, decreased after yttrium addition. The highest consumption of 0.209 mmol H_2/g was observed for non-modified HTNi catalyst. After yttrium promotion the hydrogen uptake decreased to 0.143 mmol H_2/g_{cat} and 0.151 mmol H_2/g for HTNi-Y0.2 and HTNi-Y0.4 catalysts, respectively. The decrease of reducibility has been reported before for the materials modified with higher yttrium contents of 0.6 and 1.5 wt% [3]. Fig. 3 presents TPR-H_2 profiles for studied LDHs. Two wide peaks with maxima at 386 and 829 ºC are registered for HTNi catalyst. They may be ascribed to NiO weakly-bonded to the surface of the material and nickel oxides present in the Ni-Mg-Al mixed oxides originating from layered double hydroxides, respectively [44–47]. According to Hu et al. [48] only a part of nickel can be reduced, i.e. Ni–O–Ni species, and it is not possible to reduce Ni–O–Mg. After the yttrium addition a rightward shift of the maximum temperature peak (T_{max}) was reported, which indicates stronger interaction of Ni species with the support as compared to HTNi catalyst. For HTNi-Y0.4 catalyst, the shift was less evident, as revealed in T_{max} (866 ºC).

Similar observations were reported by Huang et al. [21] for NiO-Al_2O_3 materials modified with Y_2O_3, and Y/HTNi catalysts with higher loading of yttrium [3].

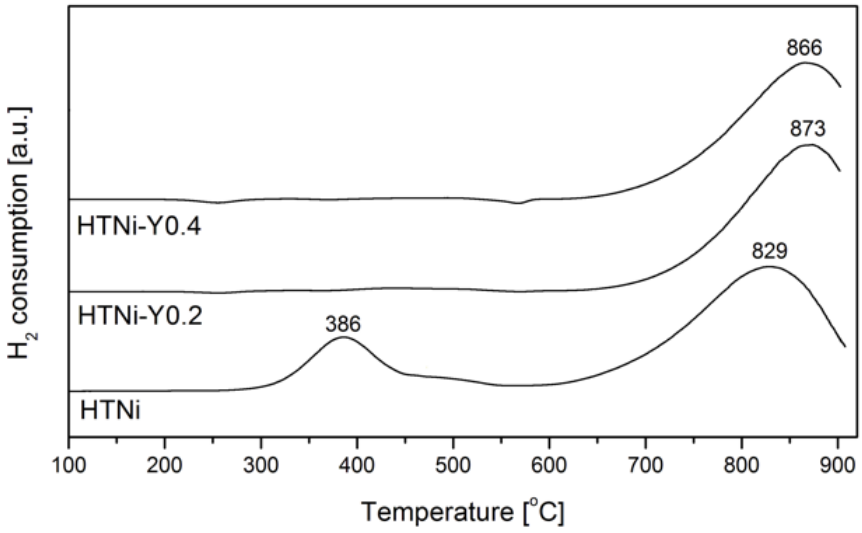

Fig. 3 TPR-H_2 profiles recorded over HTNi, HTNi-Y0.2 and HTNi-Y0.4.

Table 2 presents Ni dispersion calculated from H_2 chemisorption. There is a small increase of metallic nickel after the modification with yttrium, i.e. from for HTNi to 9.5 and 10.7 % for HTNi-Y0.2 and HTNi-Y0.4, respectively. The enhanced dispersion has been observed before in other Y modified catalysts, and it had beneficial effect on catalytic performance in DRM. Better dispersed nickel particles make them more accessible for the reaction with methane in dry reforming of methane process. The improved dispersion is linked with smaller crystal size, as confirmed by calculation assuming spherical crystallites of uniform size (Table 2). The obtained values agree well with the XRD estimates, i.e. in both characterization techniques a decrease of Ni crystallites was observed after Y promotion. A number of studies have shown that H_2 or CO chemisorption results are in line with values obtained from XRD [49–52]. This result affects the catalytic behavior of the studied materials, as will be described in the catalytic tests section.

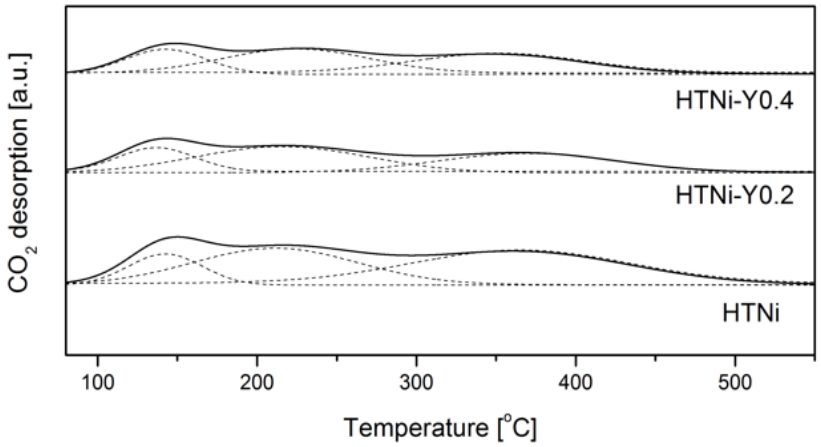

Fig. 4 TPD-CO_2 patterns recorded over the catalysts reduced at 900ºC.

Basic properties were investigated by TPD-CO_2. The results of the basicity measurements are shown in Fig. 4. Weak, medium and strong basic sites could be distinguished, respectively, with maximum peaks at the temperature range of (i) 100-150 ºC (Brønsted basic sides with surface OH^-), (ii) ca. 190 ºC (medium-strength Lewis acid-base pairings) and (iii) ca. 280 ºC (strong Lewis basic sites arising from low-coordination surface O^{2-}) [3,33,45,46,53]. Table 2 presents the calculated number of basic sites, with the highest value for HTNi catalyst. A similar value of total basicity was reported by Dębek et al. [17] and assumed as an optimal for DRM. For Y-doped catalysts this parameter decreased, being the lowest for HTNi-Y0.2. A decrease of total basicity caused by Zr, Ce or Y promotion has been reported elsewhere [3,42,54,55]. Although, the basicity was lower it did not negatively affect DRM performance of the promoted catalysts. Indeed, the modification with Zr, Ce or Y resulted in better stability and/or activity.

3.2. Catalytic tests of dry reforming of methane

A first series of experiments was performed while keeping the catalysts at certain temperatures, starting from 850 to 600 ºC. Figs. 5A-C present the CH_4 and CO_2 conversion and the H_2/CO ratio for HTNi-Y catalysts. One can find that yttrium promoted the activity of Ni-

containing layered double hydroxides. The unmodified HTNi showed the lowest values, both for CH_4 and CO_2 conversion (Figs. 5A, 5B), as well as H_2/CO molar ratio (Fig. 5C). The addition of Y significantly improved the catalytic performance. In the temperature range of 600-700 ºC the samples promoted with 0.2 and 0.4 wt.% of Y presented conversion of CO_2 higher than the one reported for the unmodified catalyst. However, an opposite effect was registered at temperatures higher than 700 ºC, in which the Y promotion led to higher CH_4 conversion. Considering the H_2/CO ratio, it was always below unity at all temperatures. The values were much higher for the Y-promoted catalysts at least in the 600-800 °C temperature range, reaching 0.98 at temperature above 750 °C.

Table 3. Side reactions occurring during dry reforming of methane.

Reaction	Equation	ΔH^{θ} [kJ/mol]
Reverse water gas shift	$CO_2 + H_2 = H_2O + CO$	41
Hydrogenation of CO_2	$CO_2 + 2H_2 = C_{(s)} + 2H_2O$	-90
Boudouard Reaction	$2\ CO = C_{(s)} + CO_2$	-172
Direct methane decomposition	$CH_4 = C_{(s)} + 2H_2$	75
Steam on C	$C_{(s)} + H_2O = CO + H_2$	131

The positive effect of the Y promotion was observed before for Ni and Y-modified Al_2O_3 [28], Y-doped Ni/SBA-15 [29,43], (Ni-Y)/KIT-6 [31], NiO-Y_2O_3-Al_2O_3 [21], Y-doped $Ce_{0.75}Zr_{0.25}O_2$ [30], and more recently, for Ni-layered double hydroxides based catalysts with higher loadings of yttrium [3]. The enhanced conversion observed for Y promoted catalysts can be directly linked with a smaller particle size of Ni° observed both by XRD and H_2 chemisorption. It is in good agreement with the appropriate values registered in this work (cp. Table 2). CO_2 conversion, which was reported to be slightly higher than that of CH_4, and the values of H_2/CO ratio lower than 1 at certain temperatures may be ascribed to the side reaction occurrence, i.e. reverse water gas-shift (RWGS) (Table 3) [21]. Moreover, when more CH_4 was

converted compared to CO_2, the other side reactions such as direct methane decomposition and Boudouard reaction could take place [45].

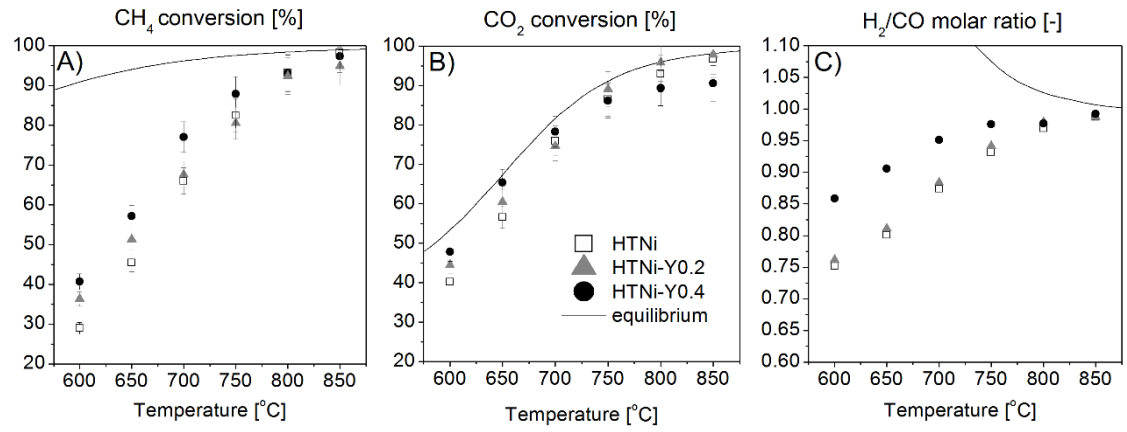

Fig. 5 Catalytic DRM tests as a function of temperature, steady-state measurements after 30 min at each temperature (GHSV=20,000 h^{-1}, $CH_4/CO_2/Ar$=1/1/8, total flow rate 100 cm^3/min^{-1}).

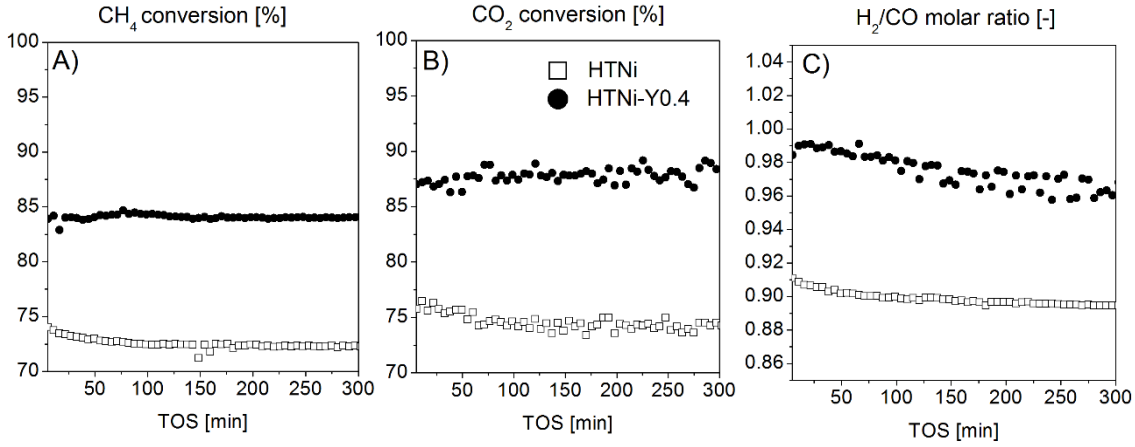

Fig. 6 Catalytic DRM tests at 700 °C (GHSV=20,000 h^{-1}, $CH_4/CO_2/Ar$=1/1/8, total flow rate 100 cm^3/min).

A second series of experiments was performed at 700 °C for 5 hours. Only HTNi-Y0.4 and HTNi were tested (after the reduction at 900 °C). The results are presented in Fig. 6. The catalytic activity of Y promoted catalyst was higher than that of HTNi. In the isothermal test,

the difference in conversion is even more marked for both CH_4 and CO_2, with CH_4 conversion of 84% for Y doped catalyst versus only 72% for the non-modified material, and CO_2 conversion of 87% for Y the doped catalyst versus only 75% for the non-doped material. In the isothermal conditions, the CO_2 conversion is still higher than CH_4 conversion, which may suggest the occurrence of RWGS (Table 3). The H_2/CO molar ratio, which is higher for Y promoted materials, is always lower than unity. The results agree with those obtained as a function of temperature (Figs. 5A, 5B, 5C). In the isothermal conditions, we clearly see that CH_4 conversion is stable after 5 h for HTNi-Y0.4 catalyst, while a slight deactivation is observed for the non-promoted material.

Based on the literature [2,10], the DRM mechanism is driven by 2 main reactions (i) decomposition of methane on nickel active site and (ii) dissociative adsorption of CO_2 on the metal surface and metal-surface interface. Promotion with yttrium resulted in the small Ni crystallite size, known to hinder direct decomposition of methane (DMD). Dissociative adsorption of CO_2 highly depends on basic properties of the catalysts. High number of strong basic sites leads to strong CO_2 adsorption which cannot further react with CH_4 molecule, and , and this, as a consequence, leads to the DMD [45]. Appropriate basicity provides good catalytic performance in dry reforming of methane, together with the suppression of carbon forming reactions. Moreover, a number of studies showed a positive effect of Y_2O_3 promotion on the rate of carbon removal due to oxygen vacancies, which induced oxygen radicals from CO_2 to react with coke [32,38,43,56,57]. Thus, a possible removal of carbon could have taken place (to some extend) according to the reverse Boudouard reaction (Table 3) [43].

In order to better understand the catalysts behavior in terms of side reactions and avoid any deactivation, the direct methane decomposition (DMD) was carried out over HTNi and HTNi-Y0.4 catalysts. The results are presented in Fig. 7, where DMD is more dominant for HTNi. During the CH_4 decomposition experiment, stable methane conversion was registered for HTNi

catalyst, whereas HTNi-Y0.4 showed decreasing values after first 30 min, pointing to an evolution of surface properties resulting in the suppression of this reaction. Small Ni crystallite size calculated for the Y-promoted sample could have contributed to this phenomenon, similar as reported in the study of Dębek et al. [41]. It illustrates that the Y promotion inhibited the direct methane decomposition, and thus the C formation.

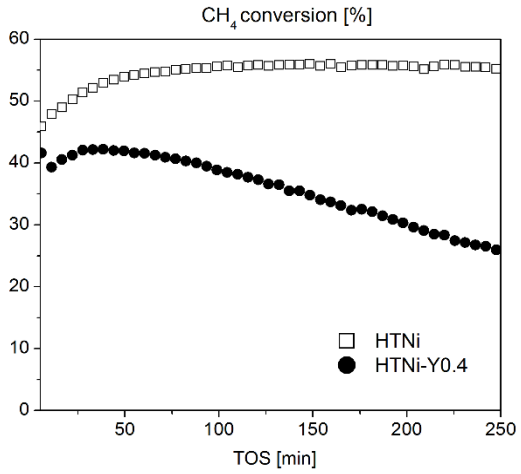

Fig. 7 Catalytic tests of direct methane decomposition as a function of temperature (GHSV=20,000 h^{-1}, CH_4/Ar=2/8, total flow rate 100 cm^3/min).

The carbon suppression has been already reported for Y-promoted materials in other studies [31,43].

3.3 Catalysts characterization after isothermal DRM tests

As reported in Table 4, the specific surface of the unpromoted spent catalyst remained constant (125 compared to 120 m^2/g), whereas the S_{BET} decreased significantly for the Y promoted spent catalyst (95 vs. 120 m^2/g). This decrease may be explained by the carbon deposition occurring upon the DRM. No changes in pore volumes and diameters of pores were registered.

Table 4. Textural and structural properties of the spent catalysts.

Catalyst	Nitrogen sorption			XRD	Raman
	S_{BET} [1)] $[m^2/g]$	V_p [2)] $[cm^3/g]$	d_p [3)] [nm]	Ni^o crystallite size [4)] [nm]	I_D/I_G
HTNi	125	0.3	10	7	1.83
HTNi-Y0.4	108	0.3	10	6	1.65

[1)] specific surface areas calculated from the BET equation

[2)] mesopore volumes derived from the BJH desorption isotherm

[3)] pore size distribution obtained from the BJH desorption isotherm

[4)] based on the Scherrer equation, from the width at half-maximum of the XRD reflections at 2Θ ca. 53°

XRD diffractograms have been recorded over the spent catalysts in order to verify the Ni° crystallite size, the possible changes in the support after the catalytic process, and the carbon formation. The results are presented in Fig. 8, where reflections typical for metallic nickel (ICOD 01-087-0712) and periclase-like mixed oxides can be found (ICOD 00-045-0946) [31,45,46,58], similarly as for the reduced samples (cp. Fig. 3). Crystallite size of Ni° did not change significantly after the tests. For both catalysts the values are close to the ones recorded for the reduced samples, i.e. 8 and 5 nm versus 7 and 6 nm for HT and HTNi-Y0.4, respectively. This suggests the lack of sintering of the nickel particles upon DRM and then confirm the stability of Y doped catalyst during DRM in stability runs. Additionally, reflections of graphite (ICOD 01-075-2078) at 2θ=26.6 ° were registered for both HTNi and HTNi-Y0.4 (Fig. 8), which shows that the studied materials have suffered a deactivation during time on stream experiments. For the HTNi catalyst additional reflections of $Mg_6Al_2(OH)_{16}CO_3 \cdot 4H_2O$ (ICOD 00-014-0191) have been registered at 2θ=11.5 ° and 22.9 °. This phase is typical for LDHs after synthesis and before calcination at around 500 °C [6,41,53]. The presence of the hydroxides (H) has been reported before for Ni-based LDHs after DRM tests, and indicates a partial

regeneration of the support in the presence of water. The latter could have been produced during side reactions, such as RWGS or hydrogenation during DRM as reported elsewhere [33,41].

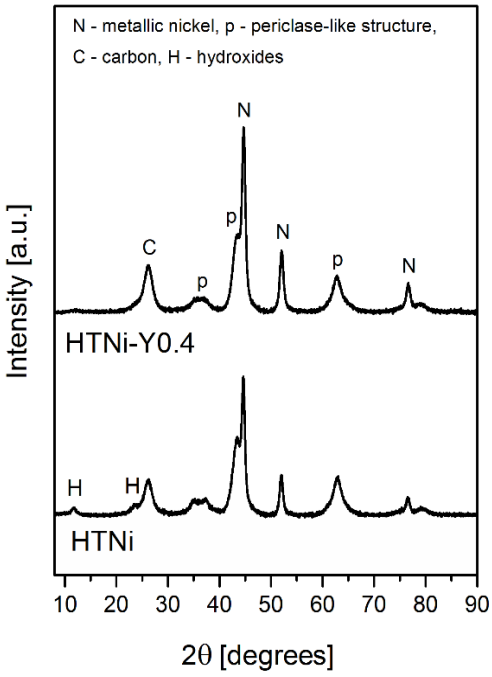

Fig. 8 XRD diffractograms of the spent catalysts (CH_4/CO_2/Ar=1/1/8, 700 ºC for 5 h).

TGA-MS data are presented in Fig. 9, where mass loss of 27% and 32% was registered for HTNi and HTNi-Y0.4, respectively. Also, a small weight increase may be observed at 300 ºC for both spent catalysts. According to Tsyganok et al. [59], this increase arises from Ni° oxidation to NiO. Moreover, the registered MS data revealed that the weight decrease was linked to CO_2 formation, which occurs due to the oxidation of carbonaceous species, formed upon dry reforming of methane [3,59,60]. The peaks of CO_2 were found at ca. 600 ºC, which mainly suggests the formation of carbon filaments [11]. Their presence was considerably higher for HTNi-Y0.4 as compared to Y-free catalyst. The formation of carbon filaments cannot be, however, linked directly with the CH_4 decomposition because of the limitation of this reaction for HTNi-Y0.4 (cp. Fig. 7).

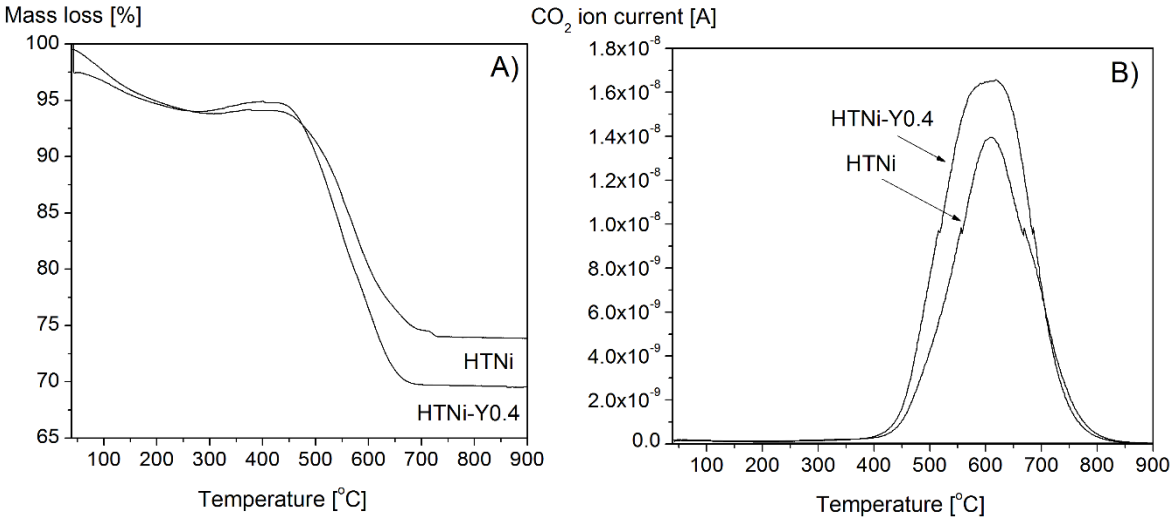

Fig. 9 TGA-MS over the spent catalyst (CH_4/CO_2/Ar=1/1/8, 700 ºC for 5 h).

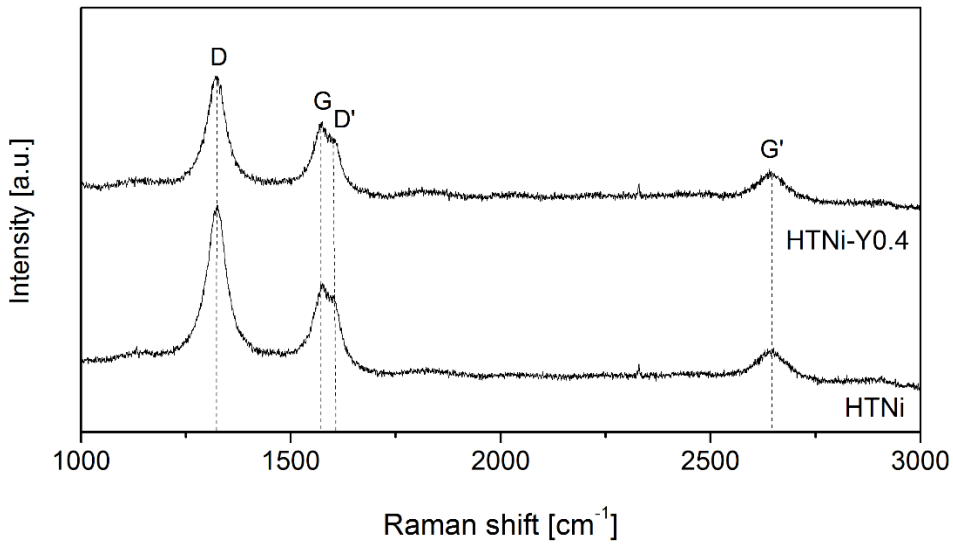

Fig. 10 Raman spectra over the spent catalysts (CH_4/CO_2/Ar=1/1/8, 700 ºC for 5 h).

Raman spectroscopy was used to examine the properties of carbonaceous species on the spent HTNi and HTNi-Y0.4 catalysts. For both materials, four bands were registered at the following Raman shift: 1324 cm^{-1} (D band), 1573 cm^{-1} (G band), 1600 cm^{-1} (D' band) and 2647 cm^{-1} (G' band) (Fig. 10). The D and D′ bands arise from a disorder present in graphite structure and they have been ascribed to the non-zone centered phonons associated to the disorder-induced vibration of C–C bond. The G and G′ bands refer to the stretching vibration in the

aromatic layers of graphite and they are only present in perfect crystalline graphite [61]. Table 4 presents the calculated ratios of I_D/I_G, which describe the graphitization degree of carbon and the disorder in its structure. The Y-modified material showed lower I_D/I_G ratio, i.e. 1.65 versus 1.83 for HTNi. One can conclude that the C deposited on Y promoted materials is more graphitic and thus more difficult to remove upon DRM [62]. This shows that low loadings of yttrium influenced the DRM mechanism in favoring side reactions, such as for example CO_2 hydrogenation. Indeed, it was observed in Figs. 6B and 6C, a slight increase in CO_2 conversion only for HTNi-Y0.4 catalyst with a simultaneous decrease of the H_2/CO ratio, showing a possible consumption of H_2 during the DRM only for the promoted catalysts.

4. Conclusions

Dry reforming of methane was studied over Ni-based layered double hydroxides precursors modified with low loadings of yttrium, i.e. 0.2 and 0.4 wt%. The catalysts were prepared by the co-precipitation method in the presence of NaOH and Na_2CO_3. In the isothermal test at 700 ºC, the promoted HTNi-Y0.4 catalyst was found to be the most active with a CH_4 conversion of ca. 84%. A slight increase in CO_2 conversion (increasing from 86.8 % to 88.4 % in 5 h time on stream test) has been also registered, together with a decrease in H_2/CO ratio. This shows a possible consumption of H_2 during the overall DRM for promoted catalyst, whereas a stable H_2/CO ratio was found for HTNi catalyst. Thus, this carbon formation could be due to CO_2 hydrogenation ($CO_2 + 2H_2 = C_{(s)} + 2H_2O$) leading to a decrease in H_2 in the gas phase and a decrease of H_2/CO ratio during DRM.

Graphitic type of carbon was recorded in the spent catalysts, which led to a decrease of the specific surface, and a greater mass loss during TGA-MS test. In the latter, CO_2 formation was recorded at 600 ºC, which suggests filamentous carbon formation. More graphitic carbon was confirmed by Raman for HTNi-Y0.4 sample than for HTNi material. However, a partial

regeneration of support has been observed and revealed as a presence of $Mg_6Al_2(OH)_{16}CO_3 \cdot 4H_2O$ reflections in XRD patterns only in the unpromoted catalyst (HTNi). This shows that Y promotion leads to a better structural resistance to the side reactions which produce H_2O, e.g. reverse-water gas shift or other reaction, such as CO_2 hydrogenation.

Acknowledgments

K. Świrk acknowledges the French Embassy in Poland for her grant "BGF Doctorat en cotutelle" between Sorbonne University and AGH University of Science and Technology. InnoEnergy PhD school and AGH (grant 15.11.210.440) are acknowledged for the financial support. This work was carried out within the framework of Erasmus+ traineeship of K. Świrk at NTNU (the KinCat Catalysis Group). T. Grzybek and M. Motak thank AGH grant 11.11.210.373.

References

[1] M.F. Mark, W.F. Maier, F. Mark, Reaction kinetics of the CO2 reforming of methane, Chem. Eng. Technol. 20 (1997) 361–370. doi:10.1002/ceat.270200602.

[2] H. Seo, Recent scientific progress on developing supported Ni catalysts for dry (CO2) reforming of methane, Catalysts. 8 (2018) 110–128. doi:10.3390/catal8030110.

[3] K. Świrk, M.E. Gálvez, M. Motak, T. Grzybek, M. Rønning, P. Da Costa, Yttrium promoted Ni-based double-layered hydroxides for dry methane reforming, J. CO2 Util. 27 (2018) 247–258. doi:10.1016/j.jcou.2018.08.004.

[4] G.K. Reddy, S. Loridant, A. Takahashi, P. Delichère, B.M. Reddy, Reforming of methane with carbon dioxide over Pt/ZrO2/SiO2 catalysts - Effect of zirconia to silica ratio, Appl. Catal. A Gen. 389 (2010) 92–100. doi:10.1016/j.apcata.2010.09.007.

[5] J. Zhang, H. Wang, A.K. Dalai, Development of stable bimetallic catalysts for carbon dioxide reforming of methane, J. Catal. 249 (2007) 300–310. doi:10.1016/j.jcat.2007.05.004.

[6] A.I. Tsyganok, M. Inaba, T. Tsunoda, S. Hamakawa, K. Suzuki, T. Hayakawa, Dry reforming of methane over supported noble metals: A novel approach to preparing catalysts, Catal. Commun. 4 (2003) 493–498. doi:10.1016/S1566-7367(03)00130-4.

[7] M.S. Fan, A.Z. Abdullah, S. Bhatia, Utilization of greenhouse gases through dry reforming: Screening of nickel-based bimetallic catalysts and kinetic studies, ChemSusChem. 4 (2011) 1643–1653. doi:10.1002/cssc.201100113.

[8] O. Muraza, A. Galadima, A review on coke management during dry reforming of methane, Int. J. Energy Res. 39 (2015) 1196–1216. doi:10.1002/er.

[9] D. Chen, R. Lødeng, A. Anundskås, O. Olsvik, A. Holmen, Deactivation during carbon dioxide reforming of methane over Ni catalyst: Microkinetic analysis, Chem. Eng. Sci. 56 (2001) 1371–1379. doi:10.1016/S0009-2509(00)00360-2.

[10] N.A.K. Aramouni, J.G. Touma, B.A. Tarboush, J. Zeaiter, M.N. Ahmad, Catalyst design for dry reforming of methane: Analysis review, Renew. Sustain. Energy Rev. 82 (2018) 2570–2585. doi:10.1016/j.rser.2017.09.076.

[11] C.E. Daza, S. Moreno, R. Molina, Co-precipitated Ni-Mg-Al catalysts containing Ce for CO2 reforming of methane, Int. J. Hydrogen Energy. 36 (2011) 3886–3894. doi:10.1016/j.ijhydene.2010.12.082.

[12] E. Alper, O. Yuksel Orhan, CO2 utilization: Developments in conversion processes, Petroleum. 3 (2017) 109–126. doi:10.1016/j.petlm.2016.11.003.

[13] R. Dębek, M. Motak, T. Grzybek, M. Galvez, P. Da Costa, A short review on the catalytic activity of hydrotalcite-derived materials for dry reforming of methane, Catalysts. 7 (2017) 32–57. doi:10.3390/catal7010032.

[14] F. Cavani, F. Trifirò, A. Vaccari, Hydrotalcite-type anionic clays: Preparation, properties and applications., Catal. Today. 11 (1991) 173–301. doi:10.1016/0920-5861(91)80068-K.

[15] A. Bhattacharyya, V.W. Chang, D.J. Schumacher, CO2 reforming of methane to syngas I: Evaluation of hydrotalcite clay-derived catalysts, Appl. Clay Sci. 13 (1998) 317–328. doi:10.1016/S0169-1317(98)00030-1.

[16] M.M. Nair, S. Kaliaguine, F. Kleitz, Nanocast LaNiO3 perovskites as precursors for the preparation of coke-resistant dry reforming catalysts, ACS Catal. 4 (2014) 3837–3846.

[17] K. Takehira, Recent development of layered double hydroxide-derived catalysts − Rehydration , reconstitution , and supporting , aiming at commercial application −, Appl. Clay Sci. 136 (2017) 112–141. doi:10.1016/j.clay.2016.11.012.

[18] Q. Zhang, T. Zhang, Y. Shi, B. Zhao, M. Wang, Q. Liu, J. Wang, K. Long, Y. Duan, P.

Ning, A sintering and carbon-resistant Ni-SBA-15 catalyst prepared by solid-state grinding method for dry reforming of methane, J. CO2 Util. 17 (2017) 10–19. doi:10.1016/j.jcou.2016.11.002.
[19] M.N. Kaydouh, N. El Hassan, A. Davidson, S. Casale, H. El Zakhem, P. Massiani, Highly active and stable Ni/SBA-15 catalysts prepared by a “two solvents” method for dry reforming of methane, Microporous Mesoporous Mater. 220 (2016) 99–109. doi:10.1016/j.micromeso.2015.08.034.
[20] J.W. Han, C. Kim, J.S. Park, H. Lee, Highly coke-resistant Ni nanoparticle catalysts with minimal sintering in dry reforming of methane, ChemSusChem. 7 (2014) 451–456. doi:10.1002/cssc.201301134.
[21] X. Huang, G. Xue, C. Wang, N. Zhao, N. Sun, W. Wei, Y. Sun, Highly stable mesoporous NiO–Y2O3–Al2O3 catalysts for CO2 reforming of methane: effect of Ni embedding and Y2O3 promotion, Catal. Sci. Technol. 6 (2016) 449–459. doi:10.1039/C5CY01171J.
[22] A. Becerra, M. Dimitrijewits, C. Arciprete, A.C. Luna, Stable Ni/Al2O3 catalysts for methane dry reforming Effects of pretreatment, Granul. Matter. 3 (2001) 79–81.
[23] L. Jin, B. Ma, S. Zhao, X. He, Y. Li, H. Hu, Ni/MgO-Al2O3 catalyst derived from modified [Ni,Mg,Al]-LDH with NaOH for CO2 reforming of methane, 3 (2017) 0–9. doi:10.1016/j.ijhydene.2017.12.087.
[24] X. Feng, J. Feng, W. Li, Insight into MgO promoter with low concentration for the carbon - deposition resistance of Ni - based catalysts in the CO2 reforming of CH4, 39 (2018) 88–98. doi:10.1016/S1872-2067(17)62928-0.
[25] N.D. Charisiou, L. Tzounis, V. Sebastian, S.J. Hinder, M.A. Baker, K. Polychronopoulou, M.A. Goula, Investigating the correlation between deactivation and the carbon deposited on the surface of Ni/Al2O3 and Ni/La2O3-Al2O3catalysts during the biogas reforming reaction, Appl. Surf. Sci. (2018). doi:10.1016/j.apsusc.2018.05.177.
[26] N.D. Charisiou, G. Siakavelas, L. Tzounis, V. Sebastian, A. Monzon, M.A. Baker, S.J. Hinder, K. Polychronopoulou, An in depth investigation of deactivation through carbon formation during the biogas dry reforming reaction for Ni supported on modified with CeO2 and La2O3 zirconia catalysts, Int. J. Hydrogen Energy. 43 (2018) 18955–18976. doi:10.1016/j.ijhydene.2018.08.074.
[27] N.D. Charisiou, A.B.V.G.P.M.A. Goula, Synthesis Gas Production via the Biogas Reforming Reaction Over Ni / MgO – Al 2 O 3 and Ni / CaO – Al 2 O 3 Catalysts, Waste and Biomass Valorization. 7 (2016) 725–736. doi:10.1007/s12649-016-9627-9.
[28] B. Li, W. Su, X. Wang, X. Wang, Alumina supported Ni and Co catalysts modified by Y2O3 via different impregnation strategies: Comparative analysis on structural properties and catalytic performance in methane reforming with CO2, Int. J. Hydrogen Energy. 41 (2016) 14732–14746. doi:10.1016/j.ijhydene.2016.06.219.
[29] B. Li, S. Zhang, Methane reforming with CO2 using nickel catalysts supported on yttria-doped SBA-15 mesoporous materials via sol-gel process, Int. J. Hydrogen Energy. 38 (2013) 14250–14260. doi:10.1016/j.ijhydene.2013.08.105.
[30] Q. Wu, J. Chen, J. Zhang, Effect of yttrium and praseodymium on properties of Ce0.75Zr0.25O2 solid solution for CH4-CO2 reforming, Fuel Process. Technol. 89 (2008) 993–999. doi:10.1016/j.fuproc.2008.03.006.
[31] K. Świrk, M.E. Gálvez, M. Motak, T. Grzybek, M. Rønning, P. Da Costa, Syngas production from dry methane reforming over yttrium-promoted nickel-KIT-6 catalysts, Int. J. Hydrogen Energy. (2018). doi:10.1016/j.ijhydene.2018.02.164.
[32] Z. Taherian, M. Yousefpour, M. Tajally, B. Khoshandam, A comparative study of ZrO2, Y2O3 and Sm2O3 promoted Ni/SBA-15 catalysts for evaluation of

CO2/methane reforming performance, Int. J. Hydrogen Energy. 42 (2017) 16408–16420. doi:10.1016/j.ijhydene.2017.05.095.
[33] K. Świrk, M.E. Gálvez, M. Motak, T. Grzybek, M. Rønning, P. Da Costa, Dry reforming of methane over Zr- and Y-modified Ni/Mg/Al double-layered hydroxides, Catal. Commun. 117 (2018) 26–32. doi:doi.org/10.1016/j.catcom.2018.08.024.
[34] L. Luo, S. Li, Y. Zhu, The effects of yttrium on the hydrogenation performance and surface properties of a ruthenium-supported catalyst, J. Serbian Chem. Soc. 70 (2005) 1419–1425. doi:10.2298/JSC0512419L.
[35] J.M. Francis, W.H. Whitlow, The effect of yttrium on the high temperatureoxidation resistance of some Fe-Cr base alloys in carbon dioxide, Corros. Sci. 5 (1965) 701–710. doi:10.1016/S0010-938X(65)80026-9.
[36] L. Ilieva, P. Petrova, G. Pantaleo, R. Zanella, J.W. Sobczak, W. Lisowski, Z. Kaszkur, G. Munteanu, I. Yordanova, L.F. Liotta, A.M. Venezia, T. Tabakova, Alumina supported Au/Y-doped ceria catalysts for pure hydrogen production via PROX, Int. J. Hydrogen Energy. (2018). doi:10.1016/j.ijhydene.2018.03.005.
[37] L. Ilieva, A. Venezia, P. Petrova, G. Pantaleo, L. Liotta, R. Zanella, Z. Kaszkur, T. Tabakova, Effect of Y Modified Ceria Support in Mono and Bimetallic Pd–Au Catalysts for Complete Benzene Oxidation, Catalysts. 8 (2018) 283. doi:10.3390/catal8070283.
[38] J.D.A. Bellido, E.M. Assaf, Effect of the Y2O3-ZrO2 support composition on nickel catalyst evaluated in dry reforming of methane, Appl. Catal. A Gen. 352 (2009) 179–187. doi:10.1016/j.apcata.2008.10.002.
[39] D.G. Mustard, C.H. Bartholomew, Determination of Metal Crystallite Supported Size and Morphology Supported Nickel Catalysts, J. Catal. 67 (1981) 186–206. doi:10.1016/0021-9517(81)90271-2.
[40] D. Wierzbicki, R. Baran, R. Dębek, M. Motak, T. Grzybek, M.E. Gálvez, P. Da Costa, The influence of nickel content on the performance of hydrotalcite-derived catalysts in CO2 methanation reaction, Int. J. Hydrogen Energy. 42 (2017) 23548–23555. doi:10.1016/j.ijhydene.2017.02.148.
[41] R. Dębek, M. Motak, D. Duraczyska, F. Launay, M.E. Galvez, T. Grzybek, P. Da Costa, Methane dry reforming over hydrotalcite-derived Ni–Mg–Al mixed oxides: the influence of Ni content on catalytic activity, selectivity and stability, Catal. Sci. Technol. 6 (2016) 6705–6715. doi:10.1039/C6CY00906A.
[42] R. Dębek, M. Motak, M.E. Galvez, T. Grzybek, P. Da Costa, Promotion effect of zirconia on Mg(Ni,Al)O mixed oxides derived from hydrotalcites in CO2 methane reforming, Appl. Catal. B Environ. (2018) 36–46. doi:10.1016/j.apcatb.2017.06.024.
[43] J.F. Li, C. Xia, C.T. Au, B.S. Liu, Y2O3-promoted NiO/SBA-15 catalysts highly active for CO2/CH4 reforming, Int. J. Hydrogen Energy. 39 (2014) 10927–10940. doi:10.1016/j.ijhydene.2014.05.021.
[44] R. Dębek, M. Motak, M.E. Galvez, T. Grzybek, P. Da Costa, Influence of Ce/Zr molar ratio on catalytic performance of hydrotalcite-derived catalysts at low temperature CO2 methane reforming, Int. J. Hydrogen Energy. 42 (2017) 1–12. doi:10.1016/j.ijhydene.2016.12.121.
[45] R. Dębek, M. Radlik, M. Motak, M.E. Galvez, W. Turek, P. Da Costa, T. Grzybek, Ni-containing Ce-promoted hydrotalcite derived materials as catalysts for methane reforming with carbon dioxide at low temperature - On the effect of basicity, Catal. Today. 257 (2015) 59–65. doi:10.1016/j.cattod.2015.03.017.
[46] H. Liu, D. Wierzbicki, R. Debek, M. Motak, T. Grzybek, P. Da Costa, M.E. Gálvez, La-promoted Ni-hydrotalcite-derived catalysts for dry reforming of methane at low temperatures, Fuel. 182 (2016) 8–16. doi:10.1016/j.fuel.2016.05.073.

[47] M. Broda, A.M. Kierzkowska, D. Baudouin, Q. Imtiaz, C. Copéret, C.R. Müller, Sorbent-enhanced methane reforming over a Ni-Ca-based, bifunctional catalyst sorbent, ACS Catal. 2 (2012) 1635–1646. doi:10.1021/cs300247g.
[48] Y.H. Hu, Solid-solution catalysts for CO2 reforming of methane, Catal. Today. 148 (2009) 206–211. doi:10.1016/j.cattod.2009.07.076.
[49] Y.J.O. Asencios, C.B. Rodella, E.M. Assaf, Oxidative reforming of model biogas over NiO-Y2O3-ZrO2 catalysts, Appl. Catal. B Environ. 132–133 (2013) 1–12. doi:10.1016/j.apcatb.2012.10.032.
[50] A.M. Venezia, L.F. Liotta, G. Pantaleo, V. La Parola, G. Deganello, A. Beck, Z. Koppány, K. Frey, D. Horváth, L. Guczi, Activity of SiO2 supported gold-palladium catalysts in CO oxidation, Appl. Catal. A Gen. 251 (2003) 359–368. doi:10.1016/S0926-860X(03)00343-0.
[51] A.L. Bonivardi, M.A. Baltanás, Preparation of Pd SiO2cfor methanol synthesis III. Exposed metal fraction and hydrogen solubility, J. Catal. 138 (1992) 500–517. doi:10.1016/0021-9517(92)90302-X.
[52] J.H. Sepúlveda, N.S. Fígoli, The influence of calcination temperature on Pd dispersion and hydrogen solubility in Pd/SiO2, Appl. Surf. Sci. 68 (1993) 257–264. doi:10.1016/0169-4332(93)90130-4.
[53] D. Wierzbicki, R. Debek, M. Motak, T. Grzybek, M.E. Gálvez, P. Da Costa, Novel Ni-La-hydrotalcite derived catalysts for CO2 methanation, Catal. Commun. 83 (2016) 5–8. doi:10.1016/j.catcom.2016.04.021.
[54] R. Dębek, M.E. Galvez, F. Launay, M. Motak, T. Grzybek, P. Da Costa, Low temperature dry methane reforming over Ce, Zr and CeZr promoted Ni–Mg–Al hydrotalcite-derived catalysts, Int. J. Hydrogen Energy. 41 (2016) 11616–11623. doi:10.1016/j.ijhydene.2016.02.074.
[55] R. Dębek, M. Motak, M.E. Galvez, P. Da Costa, T. Grzybek, Catalytic activity of hydrotalcite-derived catalysts in the dry reforming of methane: on the effect of Ce promotion and feed gas composition, React. Kinet. Mech. Catal. 121 (2017) 185–208. doi:10.1007/s11144-017-1167-1.
[56] A. Daneshmand-Jahromi, Sanaz; Reza, Rahimpour Mohammad; Meshksar, Maryam; Hafiz, Hydrogen Production from Cyclic Chemical Looping Steam Methane Reforming over Yttrium Promoted Ni/SBA-16 Oxygen Carrier, Catalysts. 7 (2017) 286. doi:10.3390/catal7100286.
[57] A.A. Lytkina, N. V. Orekhova, M.M. Ermilova, A.B. Yaroslavtsev, The influence of the support composition and structure (MXZr1-XO2-d) of bimetallic catalysts on the activity in methanol steam reforming, Int. J. Hydrogen Energy. 43 (2018) 198–207. doi:10.1016/j.ijhydene.2017.10.182.
[58] H. Shang, K. Pan, L. Zhang, B. Zhang, X. Xiang, Enhanced activity of supported Ni catalysts promoted by Pt for rapid reduction of aromatic nitro compounds, Nanomaterials. 6 (2016) 103–117. doi:10.3390/nano6060103.
[59] A.I. Tsyganok, T. Tsunoda, S. Hamakawa, K. Suzuki, K. Takehira, T. Hayakawa, Dry reforming of methane over catalysts derived from nickel-containing Mg-Al layered double hydroxides, J. Catal. 213 (2003) 191–203. doi:10.1016/S0021-9517(02)00047-7.
[60] J. Niu, S.E. Liland, J. Yang, K.R. Rout, J. Ran, D. Chen, Effect of oxide additives on the hydrotalcite derived Ni catalysts for CO2 reforming of methane, Chem. Eng. J. (2018) 0–1. doi:10.1016/j.cej.2018.08.149.
[61] I. Luisetto, S. Tuti, C. Battocchio, S. Lo Mastro, A. Sodo, Ni/CeO2-Al2O3 catalysts for the dry reforming of methane: The effect of CeAlO3content and nickel crystallite size on catalytic activity and coke resistance, Appl. Catal. A Gen. 500 (2015) 12–22.

doi:10.1016/j.apcata.2015.05.004.
[62] E. Le Saché, J.L. Santos, T.J. Smith, M.A. Centeno, H. Arellano-Garcia, J.A. Odriozola, T.R. Reina, Multicomponent Ni-CeO2 nanocatalysts for syngas production from CO2/CH4 mixtures, J. CO2 Util. 25 (2018) 68–78. doi:10.1016/j.jcou.2018.03.012.